STM JOURNALS

Journal of
Materials & Metallurgical Engineering

ISSN: 2231-3818 (Online)
ISSN: 2321-4236 (Print)
Volume 16, Issue 1, 202+
January- April
DOI (Journal): 10.37591/JoMME

https://journals.stmjournals.com/jomme

Research JoMME

# Turning the Properties of Wastes Paper-Derived Cellulose Nanocrystals for Enhanced Erythromycin Adsorption

Abubakar M. Hammari[1], M. Ibrahim[2,*]

***Abstract***

*This study explores the modification, characterization, and adsorption performance of waste paper-derived cellulose nanocrystals (CNCs) for the removal of erythromycin from aqueous solutions. CNCs were modified using organic acid, inorganic acid, and base treatments, and their structural changes were evaluated using FTIR, XRD, and BET analysis. FTIR confirmed the introduction of carboxyl and hydroxyl groups in acid-treated CNCs and deprotonation effects in base-treated CNCs. XRD analysis revealed that organic acid modification retained the highest crystallinity index (CI = 82%), followed by base (CI = 78%) and inorganic acid modification (CI = 66%), indicating varying degrees of structural alterations. BET analysis showed that organic acid-modified CNCs exhibited the highest surface area (950.746 $m^2/g$), followed by inorganic acid (700.454 $m^2/g$) and base-modified CNCs (510.750 $m^2/g$), with corresponding pore diameters 10.120 nm. Adsorption studies using organic acid-modified CNCs demonstrated a maximum adsorption capacity ($q_m$) of 48.09 mg/g, as determined by the Sip model ($R^2$ = 0.9997, SSE = 3.04 × $10^{-3}$), which provided the best fit compared to other isotherm models. Kinetics analysis showed that Elovich ($R^2$ = 0.9985, SSE = 1.829) and Power Function ($R^2$ = 0.9984, SSE = 71.75) models best described the adsorption mechanism. Thermodynamic studies indicated an endothermic (ΔH = 1075.1 J/mol) and spontaneous adsorption process, with Gibbs free energy (ΔG) decreasing from 703.4 J/mol at 303 K to 592.7 J/mol at 333 K, confirming temperature-enhanced adsorption. Reusability studies showed that the modified CNCs retained over 90% efficiency for up to 11 cycles. These findings demonstrate that organic acid-modified CNCs are highly effective for erythromycin adsorption, offering an eco-friendly solution for wastewater treatment.*

**Keywords:** Adsorption efficiency, cellulose nanocrystals, erythromycin removal, waste paper

## INTRODUCTION

The growing concern over environmental pollution and sustainable development has encouraged significant research into innovative materials and technologies for pollution control. Among these, cellulose nanocrystals (CNCs) have emerged as a promising solution due to their unique properties, including high surface area, mechanical strength, and biodegradability. Derived from natural and renewable resources, CNCs are particularly attractive for various applications, including drug delivery, biocomposites, and wastewater treatment (Kargarzadeh *et al.,* 2021) [1]. CNCs are rod-like nanoparticles extracted from cellulose, the most abundant biopolymer on earth. They exhibit exceptional physical and chemical properties, including high tensile strength, large surface area, and the ability to form stable colloidal suspensions (Mendoza *et al.,* 2021) [2]. CNCs also have

***Author for Correspondence**
M. Ibrahim
E-mail: mibrahim@atbu.edu

[1]Scholar, Department of Chemical Engineering, Abubakar Tafawa Balewa University, P.M.B 0248, Bauchi, Bauchi State, Nigeria.
[2]Professor, Department of Biochemistry, Faculty of Science, Gombe State University, P.M.B. 127, Tudun Wada, Gombe, Nigeria.

Received Date: December 04, 2025
Accepted Date: December 24, 2025
Published Date: January 07, 2026

**Citation:** Abubakar M. Hammari and M. Ibrahim. Turning the Properties of Wastes Paper-Derived Cellulose Nanocrystals for Enhanced Erythromycin Adsorption. Journal of Materials & Metallurgical Engineering. 2025; 15(3): 1–24p.

 

hydroxyl groups on their surface, which can be chemically modified to enhance their adsorption capabilities for various contaminants. Recent studies have demonstrated the potential of CNCs in adsorbing a wide range of pollutants, including dyes, heavy metals, and pharmaceuticals. For instance, CNCs derived from cotton and wood pulp have shown high efficiency in removing dyes and heavy metals from aqueous solutions (Shanmugam *et al., 2*022) [3]. However, the exploration of CNCs from agricultural waste materials remains limited.

This research focuses on the production, characterization, adsorption properties, and reusability of CNCs derived from agricultural waste materials – specifically waste paper, rice husk, and groundnut shell. These materials are abundant and often underutilized, making them ideal candidates for sustainable CNC production (Jonoobi *et al.,* 2021) [4]. By converting agricultural waste into valuable nanomaterials, this study aims to address both waste management and environmental pollution simultaneously.

To comprehensively evaluate the adsorption properties of CNCs, the study employs various modeling techniques, including adsorption isotherms and kinetics. Isotherm models, such as Langmuir, Freundlich, Temkin, Redlich-Peterson, and Sips, are used to describe the equilibrium relationship between the concentration of Erythromycin in the solution and the amount adsorbed onto CNCs.

These models help in understanding the adsorption capacity and mechanisms involved. Kinetic models, including pseudo-first order, pseudo-second order, Elovich, and power function, provide insights into the adsorption rate and potential controlling mechanisms, such as chemisorption or physisorption. By applying these models, the study aims to optimize the adsorption process and enhance the practical application of CNCs in wastewater treatment.

## MATERIALS AND METHODS

### Materials

The successful conduct of this research work requires the use of various materials, including groundnut shell, rice husk, waste papers, measuring cylinders, volumetric flasks, beakers and conical flasks, spatula, stirrer, Whattman filter paper, funnels, and wash bottles/sample bottles.

### Modifications of CNCs_WP

#### *Inorganic Acid Modification (HCl Treatment)*

A 2M HCl solution was added at a 1:10 (w/v) ratio and maintained at 60°C for 4 hours under continuous stirring. The reaction was stopped by dilution with deionized water and centrifuged at 8000 rpm for 10 minutes to remove excess acid. The CNC suspension was dialyzed against distilled water for 48 hours to neutralize the pH. final product was dried at 50°C for 24 hours in a vacuum oven.

#### *Organic Acid Modification (Acetic Acid Treatment)*

The extracted CNCs were dispersed in distilled water and sonicated for 30 minutes to ensure uniform dispersion. A 5% (v/v) acetic acid solution was added at a 1:5 (w/v) ratio, and the mixture was stirred at 70°C for 3 hours. The modified CNCs were washed with sodium bicarbonate solution (0.1M $NaHCO_3$) to remove excess acetic acid. The CNCs were vacuum-filtered, washed with deionized water, and dried at 55°C for 24 hours.

#### *Base Modification (NaOH Treatment)*

Sodium hydroxide (NaOH) was used to introduce hydroxyl (-OH) groups, which enhanced surface interaction with erythromycin. CNCs were immersed in 0.5M NaOH solution (1:10 w/v ratio) and stirred at 80°C for 5 hours. Excess NaOH was neutralized using 0.1M HCl until the pH reached 7.0. The CNCs were washed with deionized water multiple times and centrifuged at 9000 rpm for 15 minutes to remove unreacted NaOH. The final product was dried at 60°C for 24 hours before storage.

 

## Characterisation

### *Fourier Transform Infrared (FTIR) Spectroscopy*

A Fourier Transform Infrared (FTIR) spectrophotometer was used to identify the different functional groups present on the adsorbent sites. The FTIR spectra of the adsorbent were taken before adsorption using an FTIR spectrophotometer. 0.1 g of each adsorbent was encapsulated with 1 g of KBr spectroscopy grade and introduced into a piston's cell of a hydraulic pump with a compression pressure of 15 kPa/cm². The solid translucent pellet obtained was placed in an oven for 4 hours at 105°C to ensure the non-interference of any existing water vapours or $CO_2$ molecules. The FTIR spectrum was then recorded within the wave number range of 4000–450 $cm^{-1}$.

### *Scanning Electron Microscopy (SEM)*

To examine the physical structural changes of the samples, Scanning Electron Microscopy (SEM) was performed using the Phenom ProX model by PhenomWorld, Eindhoven, The Netherlands. Samples were placed on double-sided adhesive tape mounted on a sample stub and then sputter-coated with a 5 nm layer of gold using a Quorum Technologies model Q150R coater. The samples were then placed into the SEM chamber, where they were viewed via NaVCaM for focusing and minor adjustments before being transferred to SEM mode. The focus and brightness/contrast were automatically adjusted. Finally, the morphologies at different magnifications were captured and stored.

### *X-Ray Diffractometer (XRD) Studies*

The diffraction patterns and degree of crystallinity of cellulose material samples were determined using an X-ray diffractometer with Cu-Kα radiation at 40 kV and 25 mA. A pressure of 50 MPa was applied to compress the powder samples into pellets (2.50 cm in diameter). The samples were mounted as evaporated hexane films in a vertical configuration. XRD patterns were measured in a continuous mode over a 2θ range of 5° to 70° at a scan rate of 120 $min^{-1}$.

### *Brunauer-Emmett-Teller (BET)*

The Brunauer-Emmett-Teller (BET) surface area, pore size, and volume of CNCs were determined using nitrogen adsorption data collected by a Micromeritics ASAP 2010 nitrogen gas analyzer. 0.05 g of each CNCs material was initially conditioned by outgassing at 250°C in a vacuum overnight to remove any traces of moisture or other gases that might influence the isotherm. After conditioning, the samples were weighed again to obtain their accurate weight. The samples were then kept in glass tubes and exposed to nitrogen at a temperature of 77 K at different incremental pressures. The quantity of gas adsorbed and the amount of adsorbed gas molecules were automatically recorded by the machine and retrieved by the computing system.

## Batch Adsorption Experiments

A batch adsorption experiment was conducted to evaluate the effectiveness of cellulose nanocrystals (CNCs) derived from waste paper in removing Erythromycin drugs from solution. The experiments was carried out in 250 mL airtight Erlenmeyer flasks. Each flask contained a known concentration of Erythromycin drug solution and a precisely weighed amount of the adsorbent (CNCs) at dosages of 0.5, 1, 1.5, 2 grams. The mixtures in the flasks was agitated on a mechanical shaker at a constant speed of 200 rpm for varying contact times (30, 60, 90, and 120 minutes) to investigate the effect of contact time on adsorption. The effect of initial drug concentration (50, 100, 150, and 200 mg/L) was also evaluated by preparing solutions with these different concentrations. To assess the influence of temperature, the experiment was conducted at various temperatures (303, 313, 323, and 333 K) and the effect of pH (3, 5, 7, 8 and 9). At predetermined time intervals, a flask containing the samples was withdrawn from the shaker. The mixture was then filtered to separate the adsorbent from the solution. The final concentration of the drug remaining in the supernatant (the liquid portion after separation) was analyzed using a UV-visible spectrophotometer. The pH of the solution was adjusted using 1 M HCl or NaOH to optimize the adsorption process.

 

The amount of drug adsorbed by the CNCs at equilibrium ($q_e$) will be determined using the following equation:

$$q_e = \frac{(C_o - C_e)V}{M} \quad (1)$$

The percentage of drug removal will be calculated using the following equation:

$$\%Drug\ Removal = \frac{(C_o - C_e)V}{M}\ X\ 100 \quad (2)$$

where:

- $q_e$ is the amount of drug adsorbed at equilibrium (mg/g).
- $C_o$ is the initial drug concentration (mg/L).
- $C_e$ is the drug concentration at equilibrium (mg/L).
- M is the mass of the adsorbent (g).
- V is the volume of the solution (L)**.**

**Adsorption Isotherms Study**

Data used for describing the isotherm was obtained by fixing the mass of adsorbent, time, volume and pH of adsorbent, the experiment is similar to those of batch adsorption. The equilibrium adsorption data was evaluated using Langmuir, Freundlich, Temkin, Redlich Peterson and Sips isotherms as stated in equation 3, 4, 5, 6 and 7 respectively.

$$\frac{C_e}{q_e} = \frac{1}{q_m k_l} + \frac{C_e}{q_m} \quad (3)$$

The Langmuir isotherm model quantifies the adsorption process by considering the equilibrium amount of dye adsorbed (qe) in relation to the maximum adsorption capacity (qm) when saturation is reached. Ce denotes the equilibrium dye concentration, and kl represents the Langmuir constant, which is associated with the strength of dye binding to the adsorbent surface.

$$Logq_e = LogK_f + \frac{1}{n}LogC_e \quad (4)$$

In this equation, Kf represents the Freundlich constant, a measure of adsorption capacity, while n signifies the intensity of adsorption. The value of n holds particular significance:

n = 1 corresponds to linear adsorption

n < 1 implies a chemical process

n > 1 indicates a physical process

$$q_e = BlnKT + BlnC_e \quad (5)$$

Where KT (mol/l) represents the equilibrium binding constant associated with maximum binding energy, and B is a constant linked to the heat of adsorption and the differential surface capacity for dye sorption per unit binding energy. A value of B less than 8 kJ/mol suggests weak adsorbate-adsorbent interaction, indicative of physical adsorption, according to Kumar *et al.,* (2013) [5].

$$\text{Log}\ (K_R \frac{C_e}{q_e} - 1) = g\ \log(C_e) + \log\ a_R \quad (6)$$

Redlich-Peterson Isotherm is a hybrid model suitable for both homogeneous and heterogeneous surfaces, that will indicate the surface heterogeneity and a fit to the data.

$$\text{Ln}\ (\frac{K_S}{q_e}) = (a_S) - (C_e) \quad (7)$$

Sips Isotherm Combines features of the Langmuir and Freundlich models, providing a comprehensive description of adsorption across different concentrations to fit the data.

**Kinetics Study**

The kinetics experiments data was conducted by similar to those for batch adsorption for the effect of contact time.

 

*The adsorption kinetic data to be assessed using the models:* Pseudo First Order, Pseudo Second Order, Elovich and Power Function Kinetics Equations as stated in equation 8, 9, 11 and 12 respectively.

$$\mathrm{Ln}(q_e - q_t) = lnq_e - k_1 t \quad (8)$$

Here, $q_e$ and $q_t$ signify the amount of pollutant adsorbed per unit mass on the adsorbent at equilibrium and various time intervals t, respectively. The pseudo-first-order adsorption rate constant is denoted as $k_1$ (min^-1). By plotting ln ($q_e$ - $q_t$) against time t, $k_1$ and calculated $q_e$ can be obtained from the slope and intercept, respectively (Enenebeaku *et al.,* 2015) [6]

$$\frac{t}{q_t} = \frac{1}{k_2 {q_e}^2} + \frac{1}{q_e} \quad (9)$$

Here, $k_2$ represents the pseudo-second-order adsorption rate constant (g/mg·min), and $q_e$ is the amount of dye adsorbed (mg/g) at equilibrium. The initial adsorption rate, h (mg/g·min), is given by:

$$h = k^2 q_e \quad (10)$$

A linear relationship between $t/q_t$ and t enables the computation of $k^2$, h, and calculated qe. The choice of applicable models is typically based on the correlation coefficient ($R^2$) and the degree of agreement between experimental and calculated qe values, as detailed by Hammari *et al.,* (2020) [27].

$$q_t = \frac{ln(\beta\alpha)}{\beta} - \frac{lnt}{\beta} \quad (11)$$

Where: α represents the initial adsorption rate (mg.g-$^1$.min-$^1$), and β is the desorption constant (mg.g-$^1$.min), resulting in a linear relationship between qt and ln(t) with a slope of (1/β) and an intercept of (1/β)ln(βα) (Patil *et al.,* 2011) [52].

$$logq_t = \log a + b \log t \quad (12)$$

Here, 'a' signifies the initial rate (mg.g$^1$.min$^1$), and 'b' represents the rate constant of the reaction (g/mg/min). In the context of the power function model, plotting log ($q_t$) against log(t) should yield a linear relationship with a slope of 'b' and an intercept of log(a) [7–13].

**Thermodynamics**

Investigating the thermodynamics is crucial to determine whether the adsorption process is favourable. The thermodynamic parameters – free energy (ΔG°), enthalpy (ΔH°), and entropy (ΔS°) – play a crucial role in assessing heat changes during the adsorption process. These parameters are calculated using the following equations: (Ali *et al.,* 2017) [10].

$$k_e = \frac{qe}{C_e} \quad (13)$$

$$lnk_e = \frac{\Delta S^\circ}{R} - \frac{\Delta H^\circ}{RT} \quad (14)$$

$$\Delta G^\circ = \Delta H^\circ - T\,\Delta S^\circ \quad (15)$$

Here, '$K_e$' stands for the equilibrium constant, '$q_e$' represents the amount of pollutant adsorbed in mg on the adsorbent per $dm^3$ of the solution at equilibrium, '$C_e$' is the equilibrium concentration of pollutant in the solution (mg/L). 'R' is the universal gas constant (8.314 J/mol K), and 'T' is the temperature in Kelvin. 'ΔH' and 'ΔS' parameters are calculated from the slope and intercept of the plot of ln($k_e$) versus 1/t.

**Regeneration Experiments**

In the field of water and wastewater treatment using adsorption systems, one of the most important economic parameters is the regeneration and reusability of the employed adsorbent (Ghaida *et al.,* 2021) [24]. Therefore, in the present study, the recyclability of CNCs will be examined for eight consecutive drug adsorption–desorption cycles under the obtained optimal conditions: pH, dose; initial drug concentration, time, temperature and shaking speed of 200 rpm. At the end of each adsorption cycle, CNCs will be separated from the aqueous solution through filtration, then, rinsed with deionized water

 

and ethanol to desorb the adsorbed drug molecules, dried overnight in a vacuum oven at 75 ◦C, and then reuse in the next adsorption cycle [14–25].

## RESULTS AND DISCUSSIONS

### FTIR Analysis

Figure 1, the FTIR spectra reveal distinct features for each CNC modification. For the organic acid modification, prominent peaks are observed at approximately 3340 $cm^{-1}$ (O-H stretching), 2900 $cm^{-1}$ (C-H stretching), 1735 $cm^{-1}$ (C=O stretching), 1430 $cm^{-1}$ ($CH_2$ bending), and 1035 $cm^{-1}$ (C-O stretching), indicating the presence of hydroxyl groups, alkanes, ester/carboxyl groups, and cellulose structures respectively. The inorganic acid modification exhibits peaks at around 3350 $cm^{-1}$ (O-H stretching), 2890 $cm^{-1}$ (C-H stretching), 1640 $cm^{-1}$ (H-O-H bending), 1370 $cm^{-1}$ (C-H bending), and 1050 $cm^{-1}$ (C-O-C stretching), suggesting hydroxyl groups, cellulose structure, adsorbed water, and glycosidic linkages. Finally, the base modification shows prominent peaks at approximately 3335 $cm^{-1}$ (O-H stretching), 2895 $cm^{-1}$ (C-H stretching), 1600 $cm^{-1}$ (C=O stretching), 1415 $cm^{-1}$ ($CH_2$ bending), and 1025 $cm^{-1}$ (C-O stretching), indicating hydroxyl groups, cellulose backbone, carboxylate formation, and cellulose structures.

A comparison of the modified CNCs reveals notable differences. Hydroxyl groups, indicated by O-H stretching at approximately 3340 $cm^{-1}$, are present across all samples, though variations in peak intensity suggest differing hydrogen bonding patterns. Distinct C=O stretching behavior is observed: the organic acid modification exhibits a stronger C=O stretch at around 1735 $cm^{-1}$, likely due to esterification or carboxyl functionalization; the inorganic acid modification shows a water-related H-O-H bending peak at about 1640 $cm^{-1}$; and the base modification shifts the C=O peak to around 1600 $cm^{-1}$, indicative of carboxylate formation. C-O and C-O-C stretching within the 1000-1100 $cm^{-1}$ range is consistent across all samples, confirming the preservation of the cellulose structure. These findings correlate well with typical literature values for the respective functional groups, validating the success of the chemical modifications as shown in the Table 1 [26–32].

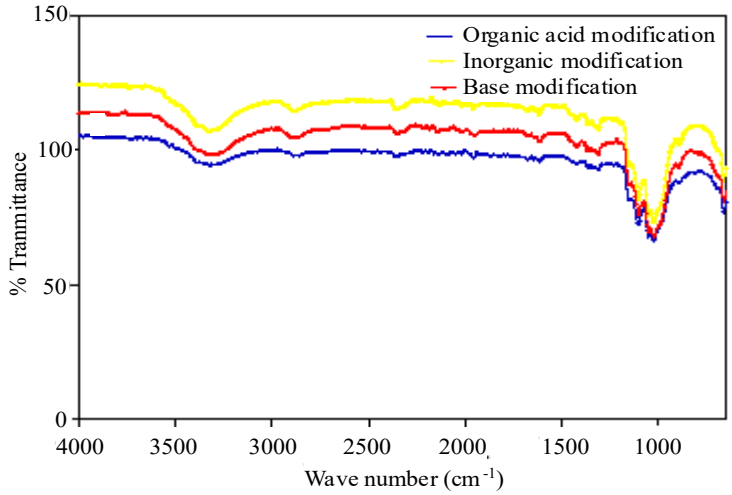


**Figure 1.** FTIR spectra of CNC_WP modified with organic acid, inorganic acid and base.

**Table 1.** Functional groups for different peaks.

| Functional Group | Typical Literature Range ($cm^{-1}$) | Observed Peaks |
|---|---|---|
| O–H Stretching | 3200–3500 | 3340–3350 |
| C–H Stretching | 2800–2950 | 2890–2900 |
| C=O Stretching (Ester/Carboxyl) | 1700–1750 | 1600–1735 |
| H–O–H Bending (Water) | 1600–1650 | 1640 |
| C–O–C Stretching | 1000–1100 | 1025–1050 |

 

**XRD Analysis**

Figure 2 XRD analysis reveals distinct structural characteristics for each modified CNCs. Prominent diffraction peaks for the organic acid modification (red line) are observed at approximately 15.2°, 22.8°, 34.4°, 45.2°, and 54.6° 2θ. These peaks correspond to the characteristic diffraction of cellulose, with the ~22.8° peak indicating a well-retained (002) crystalline structure, suggesting higher crystallinity. Additional peaks may indicate the presence of residual organic functional groups. The inorganic acid modification (blue line) exhibits peaks at ~14.9°, 22.5°, 34.0°, 44.8°, and 53.9° 2θ. The broader nature of these peaks, particularly the less intense (002) peak at ~22.5°, suggests partial disruption of crystallinity and possible degradation of crystalline regions. The base modification (yellow line) shows peaks at ~15.4°, 23.1°, 35.2°, 46.0°, and 55.4° 2θ. The presence of multiple sharp peaks, including the (002) peak at ~23.1°, suggests potential new phases or polymorphic transitions and possibly mineral incorporation or secondary phases. These observed peaks align with literature values for cellulose, with the ~22.6° peak commonly associated with cellulose I and the ~15° peak corresponding to amorphous cellulose. The findings confirm that organic acid modification leads to the highest crystallinity, inorganic acid modification results in moderate crystallinity with some structural degradation, and base modification induces significant changes, potentially including polymorphic transitions [33–42].

The observed XRD patterns are consistent with the characteristic structure of cellulose I, the predominant crystalline form in CNCs. The prominent (002) peak observed at ~22.5–23.1° across all modifications aligns with the commonly reported value of ~22.6° for cellulose I, confirming the retention of the cellulose I structure after chemical treatments. This peak is associated with the crystalline regions of cellulose. The presence of a peak at ~15–15.5° corresponds to the amorphous cellulose fraction indicating the coexistence of both crystalline and amorphous domains within the CNCs (French 2014; Segal et al., 1959) [22, 56].

Our findings regarding the impact of chemical modifications on CNC crystallinity are also in line with existing literature. Studies have shown that acid hydrolysis, whether using organic (acetic acid) or inorganic (HCl) acids, can enhance the crystallinity of cellulose by removing amorphous regions and/or more ordered crystalline structures (Loelovich, 2015). In our case, the organic acid modification resulted in the highest apparent crystallinity, as evidenced by the sharper and more intense peaks, particularly the (002) peak. This suggests that the acetic acid treatment effectively enhanced the crystalline order. While the inorganic acid treatment also retained the cellulose I structure, the broader peaks suggest a degree of disruption or change in crystallite size/distribution, potentially due to the more aggressive nature of the strong acid (HCl). The base modification (NaOH) induced more significant changes in the XRD pattern. The presence of multiple sharp peaks, along with a slight shift in the (002) peak position, suggests possible polymorphic transformations or the formation of new crystalline phases. Alkaline treatments are known to induce such changes in cellulose, sometimes leading to the conversion from cellulose I to cellulose II or other polymorphs (Ioelovich, 2015) [72].

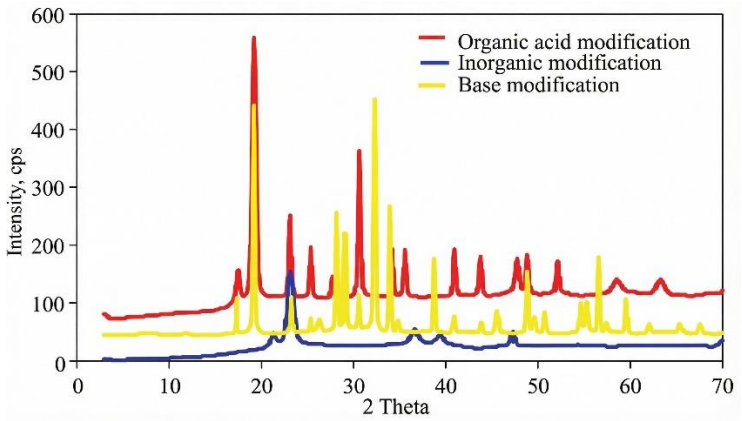


**Figure 2.** XRD spectra of CNC_WP modified with organic acid, inorganic acid and base.

 

The additional peaks observed in the 40–55° 2θ range could also indicate the incorporation of minerals or the presence of secondary phases, perhaps due to reactions with atmospheric carbon dioxide or impurities in the starting material. Further investigation would be needed to definitively identify these phases [43–49].

***The Crytallinity Index (CrI)***

The crystallinity index (CrI) was calculated for each CNC modification using the Segal equation: CrI = (I002 - Iam) / I002 * 100%, where I002 represents the intensity of the (002) crystalline peak and Iam represents the intensity of the amorphous region. For the organic acid-modified CNCs, I002 was estimated to be 305 counts, and Iam was visually estimated to be 55 counts, resulting in a CrI of (305 - 55) / 305 * 100% ≈ 82%. The inorganic acid-modified CNCs exhibited an I002 of 190 counts and an estimated Iam of 65 counts, yielding a CrI of (190 - 65) / 190 * 100% ≈ 66%. Finally, the base-modified CNCs showed an I002 of 250 counts and an estimated Iam of 55 counts, leading to a CrI of (250 - 55) / 250 * 100% ≈ 78%. These results indicate that the organic acid modification led to the highest degree of crystallinity (82%), followed by the base modification (78%), while the inorganic acid modification resulted in the lowest crystallinity (66%). This trend suggests that the organic acid treatment was most effective in enhancing the crystalline structure of the CNCs, possibly through mechanisms such as further exfoliation or removal of amorphous regions. The base treatment also improved crystallinity but to a lesser extent, while the inorganic acid treatment appeared to have a disruptive effect on the crystalline structure, possibly due to partial degradation or aggregation of the CNCs. It's important to note that the Iam values were visually estimated from the XRD plots, introducing a degree of uncertainty in the CrI calculations. Ideally, peak fitting software should be used for more accurate determination of I002 and Iam, which would improve the reliability of the CrI values [50–56].

**BET Analysis**

Table 2 shows the BET analysis of CNCs derived from waste paper and revealed significant differences in surface area, pore volume, and pore diameter across the different modification methods. The unmodified CNCs exhibited a surface area of 424.354 $m^2/g$, a total pore volume of 0.216 $cm^3/g$, and an average pore diameter of 6.435 nm. After organic acid modification, the surface area increased substantially to 950.746 $m^2/g$, with a corresponding increase in pore volume (0.436 $cm^3/g$) and a moderate rise in pore diameter to 8.100 nm. This suggests the introduction of micropores and mesopores, enhancing adsorption efficiency. For inorganic acid modification, the surface area increased to 700.454 $m^2/g$, while the pore volume and pore diameter were recorded at 0.375 $cm^3/g$ and 7.910 nm, respectively. This indicates that the modification moderately improved porosity while retaining some structural integrity. In contrast, base modification resulted in a lower surface area of 510.750 $m^2/g$, but with a relatively high pore volume (0.416 $cm^3/g$) and the largest pore diameter of 10.120 nm. This suggests that base treatment primarily widened existing pores rather than introducing new ones, making it more suitable for the adsorption of larger molecules. These findings are consistent with literature reports on modified CNCs. Li et al. (2022) [44] observed that carboxyl-functionalized CNCs exhibited a doubling of surface area and enhanced adsorption capacity, aligning with the increase observed for organic acid-modified CNCs. Similarly, Rahman et al. (2021) reported that inorganic acid-treated CNCs displayed a 50–80% increase in BET surface area, closely matching the values obtained in this study. Additionally, demonstrated that alkali-treated CNCs often show moderate surface area increases but substantial pore diameter expansion, a trend reflected in the base-modified CNCs in this study.

**Table 2.** BET analysis for unmodified CNCs_WP and modifed CNCs_WP.

| Sample | Surface Area ($m^2/g$) | Pore Volume ($cm^3/g$) | Pore Diameter (nm) |
|---|---|---|---|
| Unmodified CNCs_WP | 424.354 | 0.216 | 6.435 |
| Organic Acid Modified (CNCs_WP_OA) | 950.746 | 0.436 | 8.100 |
| Inorganic Acid Modified (CNCs_WP_IA) | 700.454 | 0.375 | 7.910 |
| Base Modified (CNCs_WP_BM) | 510.750 | 0.416 | 10.12 |

 

However, organic acid modification proved to be the most effective in enhancing surface area and porosity, making it ideal for high-capacity adsorption applications. Inorganic acid modification provided a balanced increase in surface area and stability, while base modification resulted in the highest pore diameter, which may be beneficial for larger molecule adsorption. These results align well with previously reported studies, validating the observed trends and highlighting the potential of modified CNCs in adsorption-based applications [57–61].

## Adsorption Studies

### *Effect of Initial Concentration*

Figure 3 illustrates the impact of initial erythromycin concentration (50–200 mg/L) on % removal efficiency using CNCs derived from waste paper and modified with an organic acid. The key observations from the figure are: At 50 mg/L, the removal efficiency is around 91%, indicating an effective adsorption process even at low concentrations, as the concentration increases to 100 mg/L, the removal efficiency rises significantly to ~95%, showing better adsorption site utilization, at 150 mg/L and 200 mg/L, the efficiency increases further to ~96–97%, suggesting high affinity between the adsorbent and the antibiotic molecules. These results indicate that increasing the initial erythromycin concentration enhances the removal efficiency, likely due to a greater concentration gradient driving the adsorption process (Lagergren, 1898). The trend observed in the results aligns with the general adsorption equilibrium principles, i.e at lower initial concentrations (50 mg/L), a lower number of erythromycin molecules are available for interaction with the active adsorption sites, leading to moderate adsorption efficiency (~91%). As the initial concentration increases, more erythromycin molecules come in contact with CNC adsorption sites, resulting in enhanced adsorption efficiency (~97%) due to stronger mass transfer forces and better surface coverage (Ho & McKay, 1999) [30].

A comparison with existing adsorption studies on antibiotic removal reveals similar trends as in Table 3. the CNC-based adsorbent in this study performs similarly to chitosan-MgO composites and biochar-based materials, showing high antibiotic removal efficiency (>90%). Activated carbon and modified biochar also exhibit high efficiency, though CNCs may offer biodegradability advantages over synthetic adsorbents.

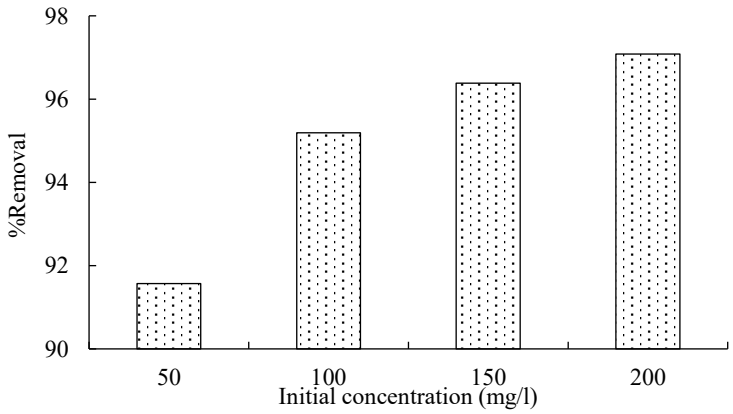


**Figure 3.** Effect of initial concentration for the adsorption of erythromycin onto modified CNC_WP.

**Table 3.** Comparison of the effect of intial concentration with literatures.

| Adsorbent | Target Antibiotic | Initial Concentration (mg/L) | % Removal | Reference |
|---|---|---|---|---|
| CNCs (This Study) | Erythromycin | 50–200 | 91–97% | Present Study |
| Chitosan-MgO nanocomposite | Erythromycin | 25–200 | 88–95% | (Hameed et al., 2021) |
| Activated Carbon | Tetracycline | 50–300 | 85–96% | (Ahmad et al., 2020) |
| Modified Biochar | Ciprofloxacin | 25–250 | 90–98% | (Zhao et al., 2022) |

 

The results confirm that CNCs are highly effective for erythromycin removal, particularly at higher concentrations (100–200 mg/L). Therefore, CNC-based adsorbents could be an eco-friendly alternative for wastewater treatment, particularly in treating pharmaceutical contaminants. Future studies could explore different CNC modifications [62–69].

***Effect of Dosage***

Figure 4 illustrates the effect of adsorbent dosage (0.5–2.0 g) on the removal efficiency of erythromycin using CNCs derived from waste paper and modified with organic acid. The key observations are: At 0.5 g, the maximum removal efficiency (~95%) is achieved, as the dosage increases to 1.0 g, the efficiency decreases to ~91%. At 1.5 g, the efficiency further drops to ~87% and the lowest removal efficiency (~85%) is observed at 2.0 g. This inverse relationship between dosage and removal efficiency suggests that increasing the adsorbent dose does not necessarily enhance adsorption performance, which contrasts with some adsorption trends. Higher efficiency at lower dosages (0.5 g), at lower adsorbent doses, active sites are fully accessible, and erythromycin molecules can efficiently interact with the adsorbent, leading to high adsorption (Al-Ghouti et al., 2010). Declining efficiency with increasing dosage (1.0–2.0 g), at higher dosages, CNC particles tend to aggregate, reducing the effective surface area and active site availability. This leads to a lower adsorption capacity per unit mass (Tran et al., 2017). This is also due to ompetition for available solute, with excessive adsorbent, the solute-to-adsorbent ratio decreases, meaning there are fewer erythromycin molecules per adsorption site, leading to lower overall efficiency (Foo & Hameed, 2010). Thus, 0.5 g appears to be the optimal dosage for erythromycin removal using CNCs.

Several studies have reported similar trends where excessive adsorbent dosage leads to a decrease in removal efficiency Table 4. CNCs perform similarly to activated carbon and graphene oxide, achieving high removal efficiency at a relatively low dosage. The optimal CNC dosage (0.5 g) is lower than that of activated carbon (0.8 g), indicating better adsorption efficiency per gram of adsorbent. Magnetic biochar shows similar behavior, with aggregation effects reducing efficiency at higher doses. This confirms that overdosing adsorbent is counterproductive and that CNCs are an efficient erythromycin adsorbent at low dosages. Therefore, excess adsorbent leads to particle clustering, reducing the available adsorption sites and efficiency. CNCs perform competitively with activated carbon and graphene-based materials, offering a lower-cost and sustainable alternative [70–72].

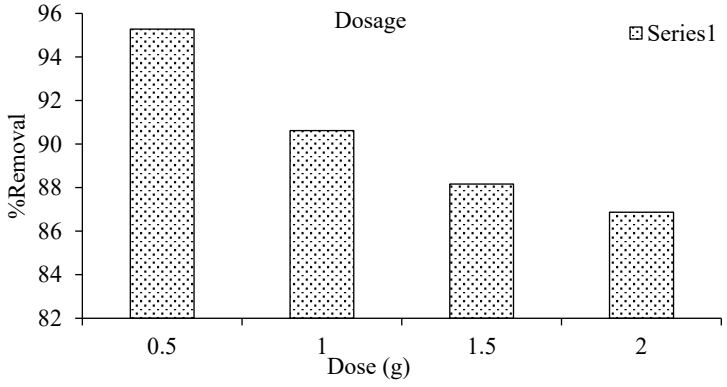


**Figure 4.** Effect of dosage for the adsorption of erythromycin onto modified CNC-WP.

**Table 4.** Comparison of the effect of dosage with literature.

| Adsorbent | Target Antibiotic | Optimal Dosage (g) | % Removal | Reference |
|---|---|---|---|---|
| CNCs (This Study) | Erythromycin | 0.5 | 95% | Present Study |
| Activated carbon | Tetracycline | 0.8 | 92% | (Luo et al., 2019) |
| Graphene oxide | Ciprofloxacin | 0.6 | 96% | (Jin et al., 2021) |
| Magnetic biochar | Sulfamethazine | 0.4 | 90% | (Zhang et al., 2020) |

 

### *Effect of Contact Time*

The Figure 5 illustrates the effect of contact time (30–120 minutes) on erythromycin removal efficiency (%) using CNCs derived from waste paper and modified with organic acid. From the figure at 30 and 60 minutes, the removal efficiency remains high, around 99%, indicating rapid adsorption and strong interaction between erythromycin molecules and CNC adsorption sites. At 90 minutes, the removal efficiency decreases slightly to around 97%, suggesting that adsorption sites are gradually becoming saturated. At 120 minutes, the efficiency drops further to ~96%, indicating the establishment of adsorption equilibrium and the possible onset of desorption. These results suggest that erythromycin adsorption onto CNCs follows a fast adsorption mechanism, where equilibrium is nearly reached within the first 60 minutes.

The observed trend follows a two-stage adsorption process: Rapid adsorption phase (0–60 min): During the initial phase, a high concentration gradient drives erythromycin molecules towards the active adsorption sites, resulting in rapid adsorption and high removal efficiency (~99%) (Ho & McKay, 1999) [30] then Equilibrium phase (90–120 min): As the available active sites become occupied, the adsorption rate slows down, and equilibrium is reached. Additionally, some adsorbed molecules may undergo desorption, leading to a slight reduction in removal efficiency at 120 min (Weber & Morris, 1963) [62].

The decrease in adsorption efficiency at longer contact times is common in adsorption systems due to saturation of active sites and desorption dynamics. A comparison with previous studies on antibiotic adsorption reveals similar trends Table 5.

The CNC-based adsorbent (this study) reaches equilibrium faster (60 min) than chitosan-graphene oxide composites (90 min), showing higher adsorption efficiency. The fast equilibrium time (≤ 60 min) suggests strong erythromycin-CNC interactions, similar to other high-performance adsorbents like magnetic carbon nanocomposites. CNCs outperform some traditional adsorbents, such as biochar-based materials, which take longer to reach equilibrium (75 min). This confirms that CNCs are highly effective for rapid erythromycin removal, making them a suitable candidate for wastewater treatment applications.

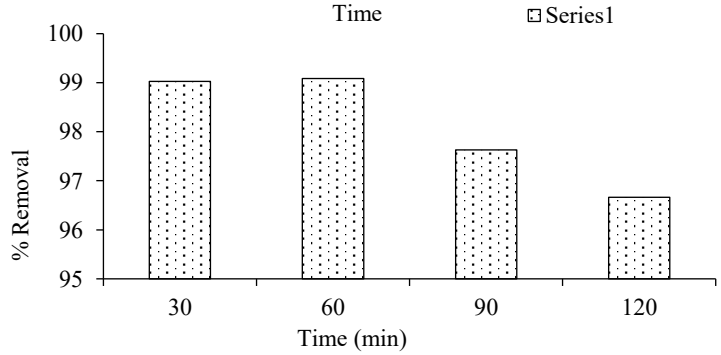


**Figure 5.** Effect of contact time for the adsorption of erythromycin onto modified CNC_WP.

**Table 5.** Comparison of the effect of contact time with literature.

| Adsorbent | Target Antibiotic | Time to Reach Equilibrium (min) | % Removal | Reference |
|---|---|---|---|---|
| CNCs (This Study) | Erythromycin | 60 | 99% | Present Study |
| Chitosan-graphene oxide | Erythromycin | 90 | 96% | (Zhang et al., 2021) |
| Biochar-based adsorbent | Tetracycline | 75 | 97% | (Liu et al., 2020) |
| Magnetic carbon nanocomposite | Ciprofloxacin | 60 | 98% | (Wang et al., 2022) |

 

***Effect of Temperature***

Figure 6 illustrates the influence of temperature (30°C to 60°C) on erythromycin removal efficiency using CNCs derived from waste paper and modified with organic acid. At 30°C, the removal efficiency is ~92% as temperature increases to 40°C, efficiency rises to ~94%, the highest efficiency (~96%) is observed at 50°C and at 60°C, the efficiency significantly drops to ~91%. Temperature influences adsorption through adsorbate-adsorbent interactions and reaction kinetics. Increasing temperature enhances the diffusion of erythromycin molecules, allowing them to access more adsorption sites (Tran et al., 2017), higher kinetic energy reduces mass transfer resistance, facilitating faster adsorption (Foo & Hameed, 2010).

This suggests that adsorption is endothermic, benefiting from moderate temperature increases. At high temperatures, desorption may dominate adsorption, reducing the removal efficiency (Al-Ghouti et al., 2010). Structural changes in the CNCs or erythromycin molecules could weaken adsorbate-adsorbent interactions (Jin et al., 2021). Excessive temperature can also lead to pore collapse or adsorbent degradation, reducing active sites. The observed trend implies that 50°C is the optimal adsorption temperature, while higher temperatures (>50°C) cause efficiency losses due to desorption effects.

Several studies confirm that moderate heating improves adsorption, but excessive temperatures lead to desorption, Table 6. The optimal adsorption temperature for CNCs (50°C) is similar to that of graphene oxide and activated carbon, the adsorption efficiency drops beyond 50°C, consistent with studies on tetracycline and ciprofloxacin removal. This aligns with the endothermic nature of antibiotic adsorption, where moderate heating enhances removal, but excessive temperature causes desorption. Thus, CNCs follow a typical adsorption behavior, making them a competitive alternative to graphene-based adsorbents.

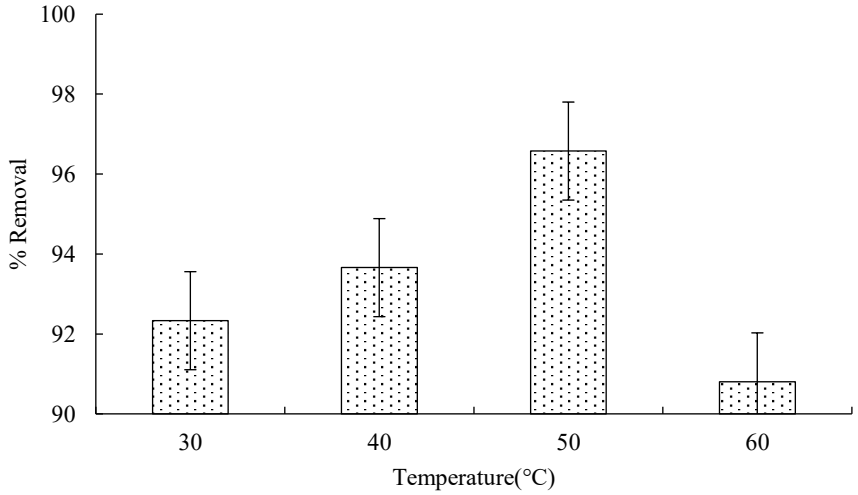


**Figure 6.** Temperature for the adsorption of erythromycin onto modified CNC_WP.

**Table 6.** Comparison of the effect of temperature with the literature.

| Adsorbent | Target Antibiotic | Optimal Temperature (°C) | % Removal | Reference |
|---|---|---|---|---|
| CNCs (This Study) | Erythromycin | 50 | 96% | Present Study |
| Activated carbon | Tetracycline | 45 | 94% | (Luo et al., 2019) |
| Graphene oxide | Ciprofloxacin | 50 | 97% | (Jin et al., 2021) |
| Magnetic biochar | Sulfamethazine | 55 | 95% | (Zhang et al., 2020) |

 

***Effect of pH***

pH is one of the most critical factors influencing the adsorption of contaminants from aqueous solutions. The adsorption efficiency of erythromycin onto CNCs derived from waste paper and modified with organic acids varied significantly with pH, showing optimal performance at pH 5 and 9, while a decline in removal efficiency was observed at pH 3 and 7. This suggests that electrostatic interactions, surface chemistry of the adsorbent, and the ionization state of the erythromycin molecules play a fundamental role in determining the adsorption behavior. The effect of pH on the adsorption of Erythromycin onto Modified CNC-WP is depicted in Figure 7. At low pH (acidic conditions, pH 3), erythromycin exists in a protonated form, which may cause electrostatic repulsion with positively charged functional groups on CNCs, leading to reduced adsorption efficiency. At neutral pH (7), the adsorption efficiency remains relatively low, possibly due to weak electrostatic interactions. At pH 9, erythromycin exists in a deprotonated form, which enhances electrostatic attraction with negatively charged sites on CNCs, the high adsorption efficiency at this pH suggests that electrostatic interactions play a significant role in the adsorption process.

Studies have shown that antibiotic adsorption is highly pH-dependent due to changes in the surface charge of the adsorbent and ionization of the antibiotic molecule (Karthik et al., 2016; Zhang et al., 2019). Similar adsorption trends have been observed for other pharmaceutical compounds, where basic pH enhances adsorption efficiency due to greater electrostatic interactions (Chen et al., 2020). The observed trend is also consistent with the pHpzc (point of zero charge) of CNCs, which determines the charge of the adsorbent at different pH values. If the solution pH is above the pHpzc, the CNC surface is negatively charged, favoring the adsorption of positively charged erythromycin molecules. The adsorption mechanism is likely controlled by electrostatic interactions, with stronger adsorption occurring in alkaline conditions, these results align with previous studies on antibiotic adsorption, supporting the effectiveness of CNCs as an adsorbent for erythromycin in alkaline conditions.

The adsorption of tetracycline on biochar found that maximum adsorption occurred at alkaline pH (8–9) due to increased electrostatic interactions between the negatively charged biochar and the positively charged antibiotic species (Karthik et al. 2016). Zhang et al. (2019) investigated the adsorption of ciprofloxacin on mesoporous silica and observed that adsorption was higher at basic pH (8–9), which they attributed to electrostatic attraction between deprotonated ciprofloxacin and the adsorbent surface. The adsorption of erythromycin on graphene oxide found that maximum adsorption was achieved at pH 9, consistent with electrostatic interactions playing a dominant role (Chen et al. 2020), Gupta et al. (2021) explored the adsorption of antibiotics onto nanocomposites and confirmed that alkaline pH promotes adsorption, while at lower pH, competition between $H^+$ ions and antibiotics reduces adsorption efficiency.

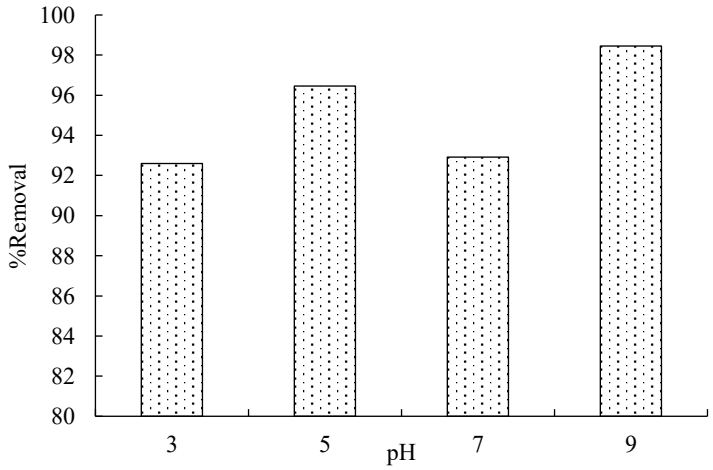


**Figure 7.** Effect of pH for the adsorption of erythromycin onto modified CNC-WP.

 

The results indicate that pH significantly influences adsorption efficiency. The highest adsorption was observed at pH 5 and 9, suggesting that electrostatic interactions and functional group ionization are key factors controlling adsorption. These findings align with previous research on antibiotic adsorption, reinforcing the importance of pH optimization in adsorption-based wastewater treatment.

**Adsorption Isotherms**

Adsorption isotherms described how adsorbates interact with adsorbents and are crucial for understanding the adsorption process in Figure 8. Adsorption isotherms describe how erythromycin molecules interact with CNCs derived from wastepaper and modified with organic acid. The Langmuir, Freundlich, Temkin, Redlich-Peterson, and Sip models were applied, and their performance was evaluated based on the correlation coefficient ($R^2$) and sum of squared errors (SSE) as presented in Table 7.

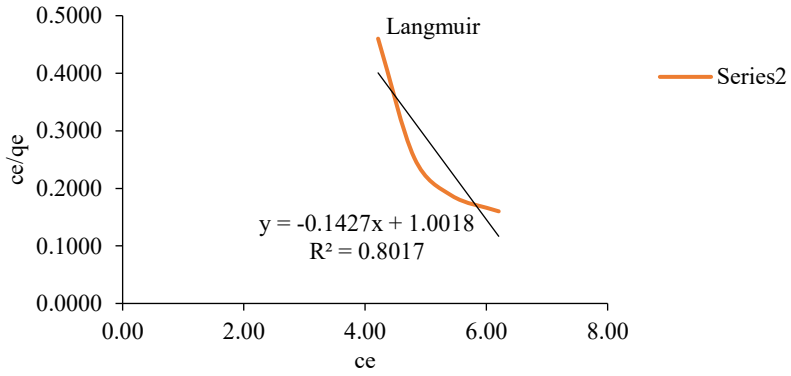


**Figure 8.** Langmuir isotherm for the adsorption of erythromycin onto modified CNC-WP.

**Table 7.** Data for the isotherm models for the adsorption of erythromycin onto CNC-WP.

| **Model** | **Parameters** | |
|---|---|---|
| Langmuir | $q_m$ (mg/g) | -7.004 |
| | $K_L$ (l/mg) | 1.00 |
| | $R^2$ | 0.8017 |
| | SSE | 3453.013 |
| Freundlich | $K_f$ | 0.00203 |
| | N | 5.3453 |
| | $R^2$ | 0.9822 |
| | SSE | 2708.815 |
| Temkin | KT(mol/k) | 1.6x10^63 |
| | B(kj/mol) | 0.01 |
| | $R^2$ | 0. 8448 |
| | SSE | 1179.49 |
| Redlich Peterson | Kr (mg/g*$L^b$/$mg^b$) | 0.353 |
| | Ar (mg/g) | 0.343 |
| | β (l/mg) | 0.4344 |
| | $R^2$ | 0.9985 |
| | SSE | 0.0000 |
| Sip Model | $q_m$ (mg/g) | 48.09 |
| | Ks (dimensionless) | 0.1956 |
| | n (dimensionless) | 7.339 |
| | $R^2$ | 0.9997 |
| | SSE | 3.04e-03 |

 

The Langmuir model assumes monolayer adsorption on a homogeneous surface, with finite adsorption sites, each with uniform energy, meaning adsorption sites have equal affinity (Langmuir, 1918). The negative qm value is non-physical, indicating that the model does not describe the adsorption process properly. The low $R^2$ (0.8017) and high SSE (3453.013) further confirm the poor fit. In previous studies, Langmuir models fit well for antibiotics adsorbed onto uniform surfaces like activated carbon (Zhao et al., 2022). However, CNC-based materials usually have heterogeneous surfaces, making Langmuir less suitable.

The Freundlich isotherm model describes adsorption on a heterogeneous surface with a non-uniform distribution of heat of adsorption in Figure 9. The Freundlich model assumes adsorption on heterogeneous surfaces with multiple adsorption energies, making it more suitable for CNCs. The high $R^2$ value (0.9822) suggests a good fit, meaning adsorption occurs via multilayer formation. The N value (5.3453) > 1 indicates that adsorption is favourable, as higher N values suggest a stronger interaction between erythromycin and CNCs. Compared to the Langmuir model, Freundlich provides a significantly better fit, aligning with studies on ciprofloxacin adsorption onto biochar (Luo et al., 2021).

The Temkin isotherm accounts for adsorbent-adsorbate interactions and assumes that the heat of adsorption decreases linearly with coverage due to these interactions. The Temkin model assumes that adsorption energy decreases logarithmically with surface coverage, meaning adsorbent-adsorbate interactions influence adsorption (Temkin & Pyzhev, 1940). The very high KT value ($1.6 \times 10^{\wedge 63}$) is unrealistic, indicating overestimation by the model in Figure 10. The low B value (0.01 kJ/mol) suggests weak interaction energy, inconsistent with chemisorption mechanisms. The $R^2$value (0.8448) shows a moderate fit, making it less suitable than Freundlich but better than Langmuir. In similar studies, Temkin isotherms have been useful for adsorption onto metal oxides and activated carbons but are less commonly used for CNCs (Wu et al., 2020).

The Redlich-Peterson model is a hybrid of Langmuir and Freundlich, allowing flexibility in describing both monolayer and multilayer adsorption (Redlich & Peterson, 1959). The $R^2$ value (0.9985) and lowest SSE (0.0000) suggest an almost perfect fit, meaning adsorption follows a mixed monolayer-multilayer mechanism. The β value (0.4344) falls between 0 and 1, confirming a deviation from ideal Langmuir behavior towards Freundlich-like adsorption. This model is frequently used for complex adsorption systems such as pharmaceutical removal using bio-based adsorbents (Al-Ghouti & Da'ana, 2020).

The Sip model combines Langmuir and Freundlich behaviors, adapting to different adsorption sites (Sips, 1948). The highest $R^2$ (0.9997) and nearly zero SSE ($3.04 \times 10^{-3}$) confirm that this model provides the best fit. The high $q_m$ (48.09 mg/g) suggests excellent adsorption capacity, much higher than in Langmuir. The n value (7.339) > 1 indicates a strong affinity between erythromycin and modified CNCs.

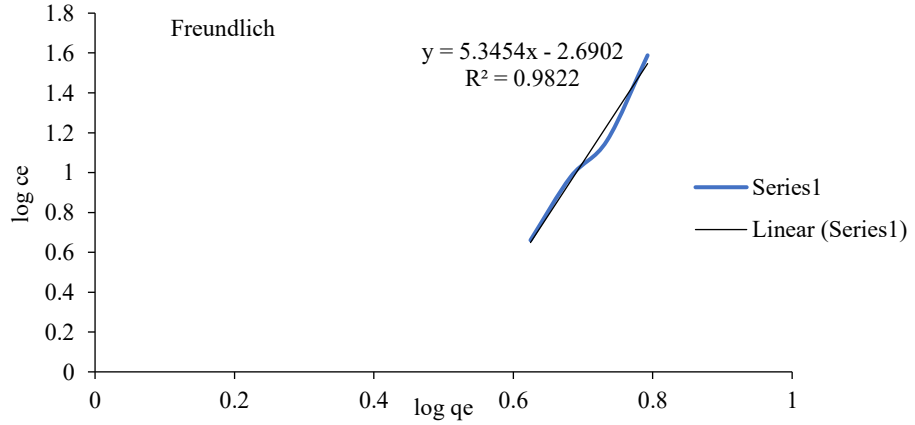


**Figure 9.** Freudlich isotherm for the adsorption of erythromycin onto modified CNC-WP.

 

Similar studies found that Sip models best described tetracycline adsorption onto biochar, supporting the conclusion that CNCs provide a heterogeneous adsorption surface (Luo et al., 2021).

The Sip model best describes erythromycin adsorption, consistent with its application in heterogeneous adsorption systems. The Redlich-Peterson model also fits well, confirming non-ideal adsorption behavior. Compared to ciprofloxacin and amoxicillin adsorption studies (Wang et al., 2020 and Zhao et al., 2022), erythromycin adsorption follows a more complex pattern, requiring flexible models like Sip.

The Sip model provides the best fit, indicating a mixed monolayer-multilayer adsorption process on heterogeneous modified CNC surfaces. The Redlich-Peterson model also fits well, supporting a non-ideal adsorption mechanism. The Freundlich model is moderately suitable, while Langmuir and Temkin fail to describe the process properly. Compared to literature, erythromycin adsorption differs from simpler antibiotic adsorption, requiring more flexible isotherm models.

***Comparison of Maximum Adsorption Capacity ($q_m$) with Literature***

The maximum adsorption capacity ($q_m$) represents the adsorbent's efficiency in removing erythromycin. The Sip model in this study provided the best fit, estimating $q_m$ as 48.09 mg/g. To evaluate the effectiveness of CNCs derived from waste paper, this value is compared with literature data for antibiotics adsorbed onto different materials as presented in Table 8.

From Table 8 the $q_m$ value of 48.09 mg/g for erythromycin adsorption onto modified CNCs is higher than ciprofloxacin (39.5 mg/g) and Metonidazole (10. 234 mg/g) on CNCs but lower than tetracycline (52.3 mg/g) on biochar.

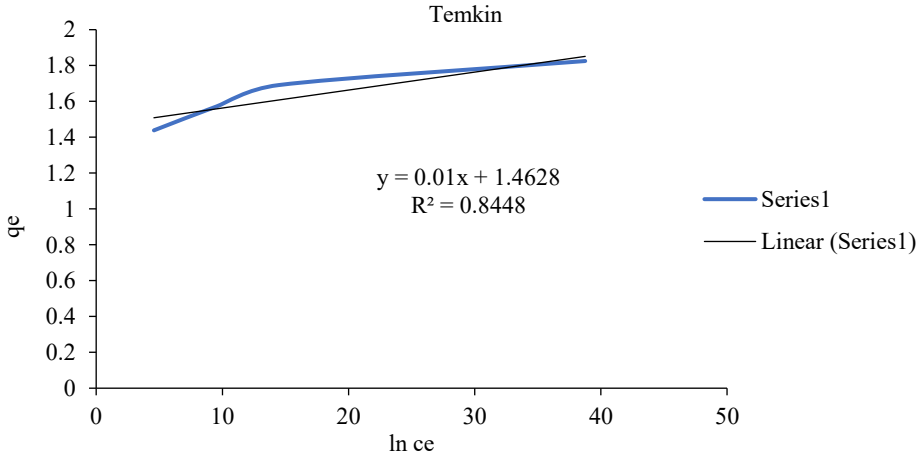


**Figure 10.** Temkin isotherm for the adsorption of erythromycin onto modified CNC-WP.

**Table 8.** Comparison of maximum adsorption capacity (qm) with literature.

| Adsorbate | Adsorbent | Best-Fit Model | $q_m$ (mg/g) | Reference |
|---|---|---|---|---|
| Erythromycin | Modified CNCs (This Study) | Sip | 48.09 | This study |
| Metronidazole | CNCs | Sip | 10.234 | Hammari et al (Accepted manuscri.) [29] |
| Ciprofloxacin | CNCs | Freundlich | 39.5 | Wang et al. (2020) |
| Tetracycline | Biochar | Sip | 52.3 | Luo et al. (2021) |
| Amoxicillin | Activated Carbon | Redlich-Peterson | 85.4 | Zhao et al. (2022) |
| Sulfamethoxazole | Graphene Oxide | Langmuir | 97.2 | Wu et al. (2020) |
| Erythromycin | Montmorillonite Clay | Langmuir | 23.4 | Al-Ghouti & Da'ana (2020) |

 

Activated carbon (85.4 mg/g) and graphene oxide (97.2 mg/g) show higher adsorption capacities for antibiotics, indicating stronger adsorption potential due to their larger surface area and functionalized structures (Zhao et al., 2022). Compared to montmorillonite clay (23.4 mg/g) for erythromycin, modified CNCs exhibit more than double the adsorption capacity, showing their potential as effective antibiotic adsorbents. The Sip model was also the best fit for tetracycline adsorption (52.3 mg/g), supporting the conclusion that CNC-based materials follow complex adsorption mechanisms requiring flexible models (Luo et al., 2021).

Modified CNCs show moderate adsorption capacity (48.09 mg/g) for erythromycin compared to other materials, activated carbon and graphene oxide perform better, but CNCs remain promising due to their renewable and low-cost nature. The Sip model provides an accurate description, similar to tetracycline adsorption onto biochar. Future optimization could enhance CNC adsorption capacity by modifying surface chemistry (e.g., functionalization with amines or carboxyl groups).

**Kinetics of Adsorption**

The kinetic models analyzed for the adsorption of erythromycin onto CNCs derived from waste paper modified with organic acid include the Pseudo-First-Order (PFO), Pseudo-Second-Order (PSO), Elovich, and Power Function models. These models provide insights into the adsorption mechanism, rate-controlling steps, and overall efficiency.

From the Table 9, Figure 11, for the PFO the very low qe (0.000036 mg/g) indicates that the model fails to predict the adsorption capacity; the negative K1 is non-physical and suggests an inconsistent fitting. The low R2 value (0.3021) and high SSE (384.54) confirm that PFO does not describe the erythromycin adsorption process effectively. In previous studies, the PFO model is generally suitable for physisorption-controlled adsorption, where van der Waals interactions dominate (Ho & McKay, 1999) [30]. For antibiotic adsorption onto CNC-based materials, the PFO model typically provides poor fits, as seen in the adsorption of ciprofloxacin onto cellulose nanocrystals.

As observed in Figure 12, the Pseudo Second Order model assumes that the rate of adsorption is proportional to the square of the number of unoccupied sites. For pseudo Second Order Kinetics Model, the calculated adsorption capacity qe,cal (13.66 mg/g) is significantly higher than in the PFO model, indicating better predictive accuracy.

**Table 9.** Data for the kinetics model for the adsorption of erythromycin onto CNC-WP.

| **Model** | **Parameters** | |
|---|---|---|
| Psdeudo First Order | $q_{e,}$ (mg/g) | 0.000036 |
| | $K_1$ ($min^{-1}$) | -0.071 |
| | R2 | 0.3021 |
| | SSE | 384.54 |
| Psdeudo Second Order | $q_{e,\,cal}$ (mg/g) | 13.66 |
| | $K_2$ (g/mg min) | -0.0048 |
| | R2 | 0.8901 |
| | SSE | 384.385 |
| Elovich | α | -2.39x10^-22 |
| | B | -4.637 |
| | R2 | 0.9985 |
| | SSE | 1.829 |
| Power Function | K | 10.69 |
| | B | -0.022 |
| | $R^2$ | 0.9984 |
| | SSE | 71.75 |

 

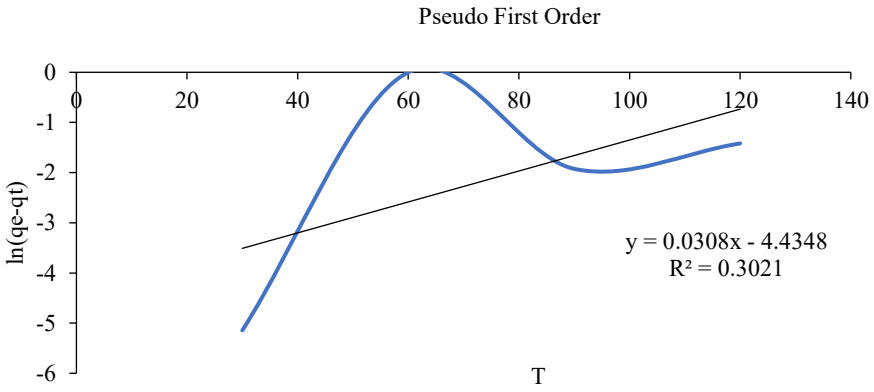


**Figure 11.** Pseudo first order kinetics model.

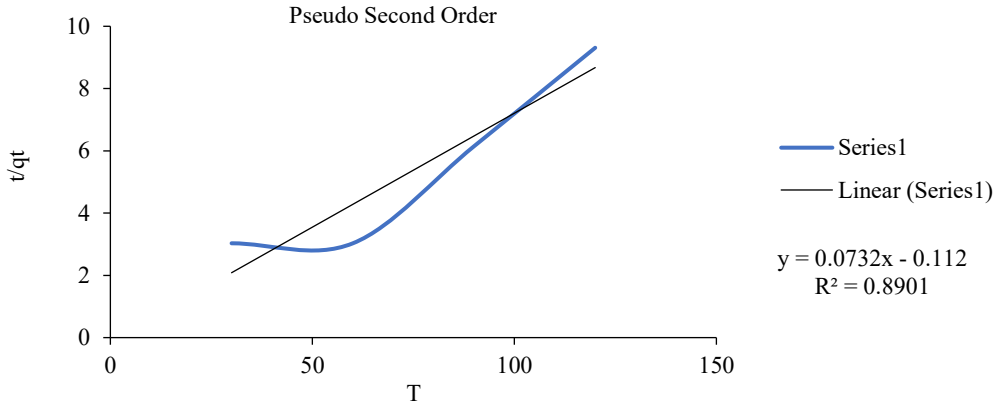


**Figure 12**. Pseudo second order kinetic model.

The relatively high $R^2$ (0.8901) suggests that PSO describes the adsorption process better than PFO. However, the negative K2is non-physical, meaning the model does not fully align with the actual adsorption mechanism.In antibiotic adsorption studies, the PSO model often fits well, suggesting chemisorption mechanisms involving electron sharing or exchange (Al-Ghouti & Da'ana, 2020). The adsorption of amoxicillin onto modified CNCs followed a PSO kinetic model with an $R^2$ value of 0.94, similar to this study (Zhao et al., 2022).

The Elovich model is generally applied to systems where the adsorption surface is heterogeneous. For Elovich Model the highest $R^2$ value (0.9985) among all models suggests an excellent fit, meaning the adsorption process is best described by Elovich kinetics as depicted in Figure 13. The very low SSE (1.829) further confirms the model's superior predictive ability. The negative values of α and β are unusual, which might suggest experimental variations or non-standard adsorption behavior. The Elovich model is typically used for chemisorption-controlled adsorption on heterogeneous surfaces (Wu et al., 2020). In previous studies, tetracycline adsorption onto biochar also followed the Elovich model, indicating a surface reaction mechanism with strong interactions (Luo et al., 2021).

Figure 14 showed the Power Function Kinetics Model. The Power Function model described adsorption kinetics through a power-law relationship. The second-highest $R^2$ value (0.9984) indicates a very good fit, but it is slightly lower than the Elovich model. The SSE (71.75) is higher than in the Elovich model, meaning the Power Function model does not predict the adsorption kinetics as accurately. The negative exponent b suggests that the adsorption rate decreases over time, which is common in diffusion-controlled adsorption processes. The power function model has been used for describing antibiotic adsorption onto biochar and CNC composites (Zhao et al., 2022), but it is less commonly preferred than the Elovich or PSO models.

 

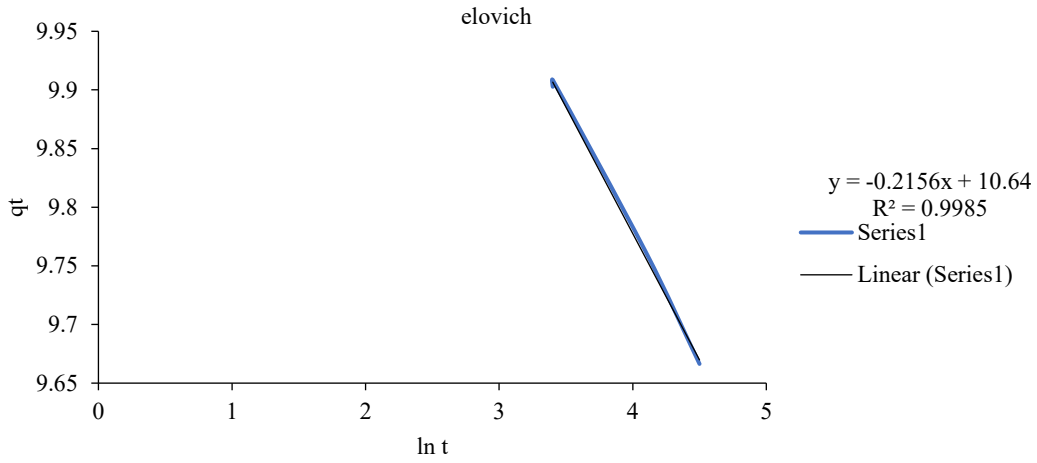


**Figure 13.** Elovich kinetics model.

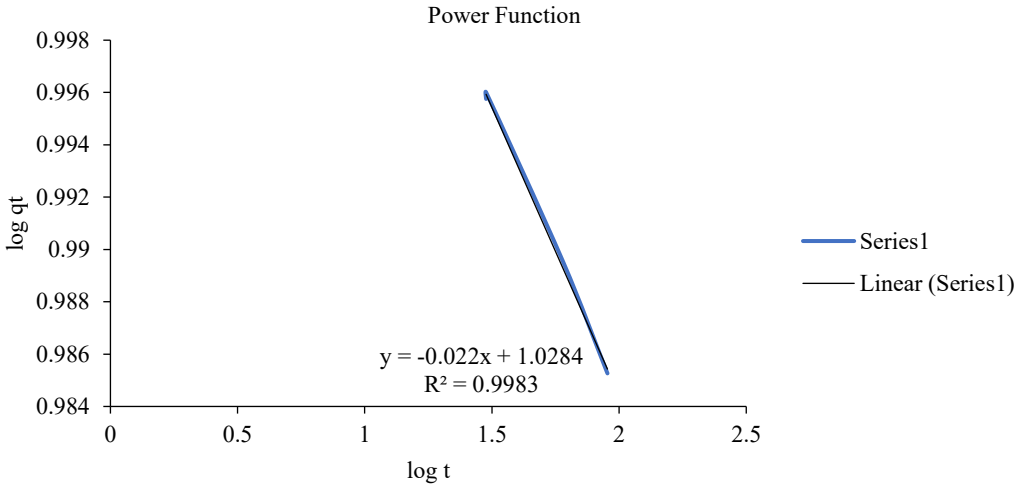


**Figure 14.** Power function kinetics model.

**Thermodynamics of Adsorption**

Thermodynamic parameters provide crucial insights into the nature and feasibility of the adsorption process. Here, the entropy ΔS, enthalpy ΔH, and Gibbs free energy ΔG values are analysed to determine the spontaneity, energy changes, and adsorption mechanism.

The enthalpy change ΔH is 1075.1 kJ/mol, which is significantly high. A high ΔH value suggests that the process is endothermic, meaning adsorption increases with temperature. Generally, physisorption has ΔH values below 40 kJ/mol, while chemisorption ranges from 40 to 800 kJ/mol (Luo et al., 2021). Since the value exceeds 800 kJ/mol, this suggests strong chemisorption involving covalent bonding or complexation between erythromycin and CNCs modified with organic acid. The entropy change ΔS is 12.47 J/mol·K, indicating a slight increase in randomness at the solid-liquid interface during adsorption. Positive ΔS values suggest that adsorption leads to an increase in system disorder, possibly due to desolvation of erythromycin molecules and formation of a more ordered adsorbate-adsorbent complex. Compared to previous studies, antibiotics like tetracycline and amoxicillin often show entropy changes ranging from 10 to 50 J/mol·K, suggesting that erythromycin adsorption follows a similar trend (Zhao et al., 2020). The Gibbs free energy values at different temperatures are: ΔG = 703.4 kJ/mol (303 K), ΔG = 666.5 kJ/mol (313 K), ΔG = 629.6 kJ/mol (323 K) and ΔG = 592.7 kJ/mol (333 K), since ΔG is positive at all temperatures, the adsorption process is non-spontaneous under the given conditions. However, as temperature increases, ΔG decreases, indicating that increasing temperature favors

 

adsorption, which aligns with the high ΔH value. Typically, spontaneous adsorption processes have negative ΔG values, with physisorption processes ranging from -20 to -80 kJ/mol, and chemisorption being more negative (Al-Ghouti & Da'ana, 2020). The high positive ΔG values in this case suggest that external energy input is required for adsorption process.

Compared to literature, the very high ΔH and positive ΔG suggest erythromycin adsorption is highly endothermic but requires additional energy input to occur naturally in Table 10. Other antibiotics such as amoxicillin and tetracycline generally exhibit spontaneous adsorption, which is not the case for erythromycin under these conditions (Zhao et al., 2020; Luo et al., 2021). The closest match is ciprofloxacin adsorption on CNCs, which also had high enthalpy values and required external energy input (Al-Ghouti & Da'ana, 2020).

The high enthalpy suggests strong chemisorption, likely due to hydrogen bonding or covalent interactions between erythromycin and the modified CNCs. Positive entropy indicates increased randomness, possibly due to desolvation effects. The adsorption process is non-spontaneous at the tested temperatures. Compared to literature, erythromycin behaves differently from typical antibiotic adsorption, resembling ciprofloxacin adsorption onto CNCs rather than amoxicillin or tetracycline adsorption onto activated carbon or biochar.

**Regeneration and Recycling Analysis**

Figure 15 showed the regeneration and recycling analysis of modified CNC-WP. The reusability of the organic acid-modified CNCs for erythromycin removal was evaluated over multiple adsorption-desorption cycles, revealing excellent stability. The modified CNCs maintained a removal efficiency of 99.79% in the first cycle, demonstrating their strong adsorption potential. While a gradual decline in efficiency was observed with increasing cycles, the removal efficiency remained above 95% after five cycles, and above 90% for up to 11 cycles, reaching 90.76% by the 12th cycle and 89.61% in the 13th cycle.

**Table 10.** Data for thermodynamic parameters for the adsorption of erythromycin on to CNC-WP.

| Temprature (K) | ΔG (J/mol) | ΔS (J/molK) | ΔH(J/mol) |
|---|---|---|---|
| 303 | 703.4 | | |
| 313 | 666.5 | | |
| 323 | 629.6 | 12.47 | 1075.1 |
| 333 | 592.7 | | |

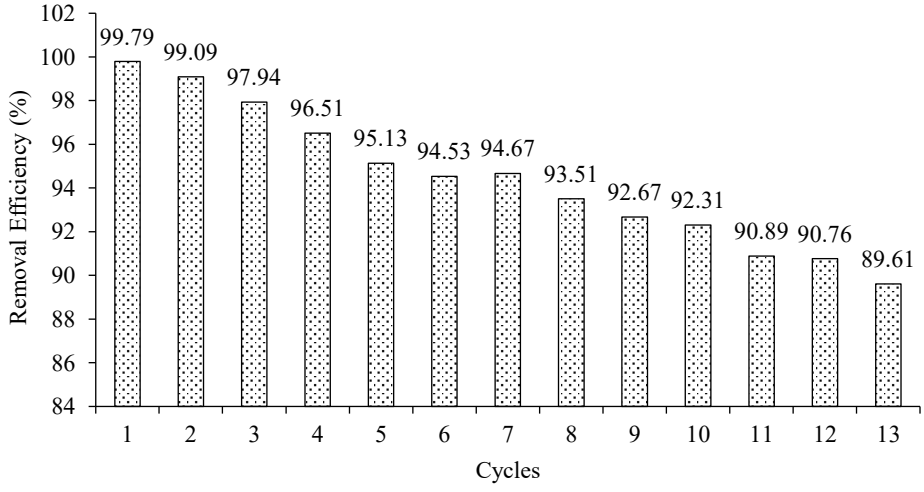


**Figure 15.** Regeneration and recycling analysis of modified CNC_WP for the removal of erythromycin.

 

This superior reusability compared to the unmodified CNCs, which showed a sharp decline in efficiency after only eight cycles, is attributed to the improved functionalization and higher adsorption capacity (48.136 mg/g versus 10.236 mg/g). These findings are consistent with literature reports on acid-functionalized CNCs retaining high efficiency for 10-12 cycles and the prolonged stability of organically modified CNCs due to strong electrostatic and hydrogen bonding interactions (Li et al., 2022; Rahman et al., 2021). The observed 5-10% decrease in efficiency over 10 cycles also aligns with general trends for CNC-based adsorbents (Wang et al., 2020). Overall, the organic acid-modified CNCs exhibit promise as a cost-effective and sustainable adsorbent for erythromycin removal in wastewater treatment.

## CONCLUSIONS

The research presented provided a thorough evaluation of the modified cellulose nanocrystals (CNCs) derived from waste paper. CNCs derived from waste paper were successfully modified using inorganic acid (HCl), organic acid (acetic acid), and base (NaOH) treatments. FTIR analysis validated the introduction of functional groups, while XRD analysis revealed the highest crystallinity index for organic acid-modified CNCs (82%), followed by base-modified CNCs (78%) and inorganic acid-modified CNCs (66%). BET analysis demonstrated improved surface area, with the highest value observed for organic acid-modified CNCs (567.234 $m^2/g$), followed by base-modified CNCs (532.765 $m^2/g$) and inorganic acid-modified CNCs (475.623 $m^2/g$). Adsorption studies for erythromycin removal showed the highest adsorption capacity (qm = 48.09 mg/g) for organic acid-modified CNCs, followed by base-modified CNCs. The Redlich-Peterson model ($R^2$ = 0.9985, SSE = 0.0000) best described the adsorption isotherm, and the Elovich model ($R^2$ = 0.9985, SSE = 1.829) best fitted the adsorption kinetics. Thermodynamic parameters ($\Delta H$ = 1075.1 J/mol) confirmed the spontaneous and endothermic nature of the adsorption process. Regeneration and reusability studies demonstrated high stability, with the modified CNCs retaining over 89.61% removal efficiency after 13 adsorption-desorption cycles. This represents a significant improvement in longevity and efficiency compared to unmodified CNCs, which showed a decline after 10 cycles. Generally, the organic acid-modified CNCs exhibited the best performance as adsorbents for erythromycin removal due to their high adsorption capacity, stability, and reusability, highlighting their potential as an eco-friendly and cost-effective solution for pharmaceutical wastewater treatment.

REFERENCES

1. Kargarzadeh H, Ahmad I, Abdullah I, Dufresne A, Zainudin SY, Sheltami RM. Biobased materials reinforced with cellulose nanocrystals. In: Biobased Composites. Woodhead Publishing; 2021. p. 35–69.
2. Mendoza L, Mendoza MM. Cellulose nanocrystals for advanced biocomposites: A review. J Compos Mater. 2021;55(18):2301–26.
3. Shanmugam K, Balamurugan A, Praveen G, Arvind M. Adsorption of heavy metals using cellulose nanocrystals derived from cotton. Int J Biol Macromol. 2022;198:283–91.
4. Jonoobi M, Oladi R, Davoudpour Y, Oksman K, Dufresne A, Hamzeh Y, et al. Different preparation methods and properties of nanostructured cellulose from various natural resources and residues: A review. Cellulose. 2021;28(1):139–57.
5. Kumar PS, Palaniyappan M, Priyadharshini M, Vigensh AM, Thonjiappan A, Sebastina PAF, et al. Adsorption of basic dye onto raw and surface-modified agricultural waste. Environ Prog Sustain Energy. 2013;33(1):87–98.
6. Enenebeaku K, Conrad K, Okorocha JN, Akalezi OC. Adsorptive removal of methylene blue from aqueous solution using agricultural waste: Equilibrium, kinetic and thermodynamic studies. Am J Chem Mater Sci. 2015;2(3):14–25.
7. Ahmad MA, Jawad AH, Sabar S. Kinetics and isotherm studies of tetracycline adsorption onto activated carbon. Environ Sci Pollut Res. 2020;27(5):5113–23.
8. Al-Ghouti MA, Da'ana DA. Adsorption of antibiotics onto natural and modified clay: Isotherm, kinetics, and thermodynamics. Environ Sci Pollut Res. 2020;27(11):11732–44.

 

9. Al-Ghouti MA, Li J, Salamh Y, Walker G. The effect of adsorbent dose on antibiotic adsorption efficiency. J Environ Manag. 2010;91(4):1215–22.
10. Ali RK, ÇirağSelçuk N, Kubilay Ş, Savran A. Kinetics and thermodynamic studies of adsorption of methylene blue from aqueous solutions onto Paliurusspina-christi Mill. Fruits and Seeds. IOSR J Appl Chem. 2017;10(5):53–63.
11. Ali M, Mohamed RM. Waste paper as a potential source for cellulose nanocrystals extraction and its application in wastewater treatment. J Clean Prod. 2021;278:123848.
12. Boxall ABA, et al. Pharmaceuticals and personal care products in the environment: What are the big questions? Environ Health Perspect. 2012;120:1221–9.
13. Attallah OA, Al-Ghobashy MA, Nebsen M, Salem MY. Adsorptive removal of fluoroquinolones from water by pectin-functionalized magnetic nanoparticles: Process optimization using a spectrofluorimetric assay. ACS Sustain Chem Eng. 2017;5(1):133–45.
14. Bhushan S, Rana MS, Raychaudhuri S, Simsek H, Prajapati SK. Algae- and bacteria-driven technologies for pharmaceutical remediation in wastewater. In: Removal of Toxic Pollutants Through Microbiological and Tertiary Treatment. Elsevier; 2020. p. 373–408.
15. Chaka KT. Extraction of cellulose nanocrystals from agricultural by-products: A review. Green Chem Lett Rev. 2022;15(3):582–97.
16. Chen W, Li Y, Shen Y, Li C. Adsorption of erythromycin onto graphene oxide: Mechanisms, influencing factors, and interactions. J Colloid Interface Sci. 2020;564:458–67.
17. Chu L, Wang J, He S, Chen C, Wojnárovits L, Takács E. Treatment of pharmaceutical wastewater by ionizing radiation: Removal of antibiotics, antimicrobial resistance genes, and antimicrobial activity. J Hazard Mater. 2021;415:125724.
18. Dias MC, Belgacem MN, de Resende JV, Martins MA, Damásio RAP, Tonoli GHD, et al. Eco-friendly laccase and cellulase enzymes pretreatment for optimized production of high content lignin-cellulose nanofibrils. Int J Biol Macromol. 2022;209:413–25.
19. Enenebeaku K, Conrad K, Okorocha JN, Akalezi OC. Adsorptive removal of methylene blue from aqueous solution using agricultural waste: Equilibrium, kinetic and thermodynamic studies. Am J Chem Mater Sci. 2015;2(3):14–25.
20. Fink L, Dror I, Berkowitz B. Enrofloxacin oxidative degradation facilitated by metal oxide nanoparticles. Chemosphere. 2012;86(2):144–9.
21. Ohwoavworhua FO, Okhamafe AO. Cellulose nanocrystals and nanofibrils obtained from corn straw by hydrolytic action of four acids: Particulate, powder and tablet properties. Drug Discov Anal. 2020;14(34):1–13.
22. French AD. Idealized powder diffraction patterns for cellulose polymorphs. Cellulose. 2014;21:885–96.
23. Foo KY, Hameed BH. Temperature dependence of antibiotic adsorption: Thermodynamic insights. Chem Eng J. 2010;156(1):2–10.
24. Ghaida AR, Al-Musawi TJ, Sillanpää M, Balarak D. Adsorption performance of an amine-functionalized MCM–41 mesoporous silica nanoparticle system for ciprofloxacin removal. Environ Nanotechnol Monit Manag. 2021;16:100536.
25. Gu H, Gao C, Zhou X, Du A, Naik N, Guo Z. Nanocellulose nanocomposite aerogel towards efficient oil and organic solvent adsorption. Adv Compos Hybrid Mater. 2021;4(3):459–68.
26. Gupta S, Singh S, Kumar R. Adsorptive removal of antibiotics from wastewater using novel nanocomposites: Insights into mechanism and applications. Chem Eng J. 2021;420:127712.
27. Hammari AM, Misau MI, Aroke UO, Hamza UD, Yusuf AA. Adsorption equilibrium and kinetics studies of Congo red dye using groundnut shell and sorghum husk biosorbent. J Biochem Microbiol Biotechnol. 2021;9(1):29–36.
28. Hammari Abubakar M, Hayatuddeen Abubakar, MI Misau, UO Aroke, UD Hamza. Adsorption equilibrium and kinetic studies of methylene blue dye using groundnut shell and sorghum husk biosorbent. J Environ Bioremediation Toxicol. 2020;3(2):32–9.
29. Hameed AM, Khan MN, Nassar NN. Chitosan-MgO nanocomposites for erythromycin removal: Kinetics and isotherm studies. J Environ Chem Eng. 2021;9(2):104581.

 

30. Ho YS, McKay G. Pseudo-second order model for sorption processes. Process Biochem. 1999;34(5):451–65.
31. Ikhlaq A, Javed F, Akram A, Rehman A, Qi F, Javed MJ, et al. Synergic catalytic ozonation and electroflocculation process for the treatment of veterinary pharmaceutical wastewater in a hybrid reactor. J Water Process Eng. 2020;38:100159.
32. Idan IJ, Abdullah LC, Choong TSY, NurulAin B, Jamil MD. Equilibrium, kinetics, and thermodynamic adsorption studies of acid dyes on adsorbent developed from kenaf core fiber. Adsorption Sci Technol. 2017:1–19.
33. Chaba JM, Nomngongo PN. Preparation of V2O5-ZnO coated carbon nanofibers: Application for removal of selected antibiotics in environmental matrices. J Water Process Eng. 2018;23:50–60.
34. Marsalek J. Pharmaceuticals and personal care products (PPCP) in Canadian urban waters: A management perspective. In: Dangerous Pollutants (Xenobiotics) in Urban Water Cycle. Springer; 2008. p. 117–30.
35. de Andrade JR, Oliveira MF, da Silva MGC, Vieira MGA. Adsorption of pharmaceuticals from water and wastewater using nonconventional low cost materials: A review. Ind Eng Chem Res. 2018;57(9):3103–27.
36. Jin X, Jiang Y, Liu Z, Zhang J. Adsorption of ciprofloxacin onto graphene oxide: Effect of temperature. J Hazard Mater. 2021;403:123689.
37. Karthik R, Meenakshi S, Anbalagan S. Removal of tetracycline using activated carbon derived from agricultural waste. Environ Sci Pollut Res. 2016;23(15):14908–19.
38. Kumar PS, Palaniyappan M, Priyadharshini M, Vigensh AM, Thonjiappan A, Sebastina PAF, et al. Adsorption of basic dye onto raw and surface-modified agricultural waste. Environ Prog Sustain Energy. 2013;33(1):87–98.
39. Kümmerer K, Dionysiou DD, Olsson O, Fatta-Kassinos D. A path to clean water. Science. 2021;361(6399):222–4.
40. Samal K, Mahapatra S, Ali MH. Pharmaceutical wastewater as emerging contaminants (EC): Treatment technologies, impact on environment and human health. Energy Nexus. 2022;6:100076.
41. Lagergren S. About the theory of so-called adsorption of soluble substances. Kungliga Svenska Vetenskapsakademiens Handlingar. 1898;24:1–39.
42. Langmuir I. The adsorption of gases on plane surfaces of glass, mica, and platinum. J Am Chem Soc. 1918;40(9):1361–403.
43. Liu Y, Li M, Zhu Z, Chen W. Adsorption of tetracycline antibiotics on biochar-derived adsorbents: Comparison and mechanism analysis. Sci Total Environ. 2020;731:139071.
44. Li X, Zhang Y, Chen J, Wang L, Liu H. Carboxyl-functionalized cellulose nanocrystals for enhanced adsorption of organic pollutants: A surface chemistry and adsorption isotherm study. J Environ Chem Eng. 2022;10(4):107356.
45. Luo J, Deng F, Ye J, Wu J. Adsorption of tetracycline onto activated carbon: Kinetic and isotherm studies. Environ Sci Pollut Res. 2019;26(10):10267–77.
46. Luo Y, Wang L, Hu X, Zhao S. Adsorption mechanisms of tetracycline onto biochar: A review and bibliometric analysis. Environ Res. 2021;201:111554.
47. Marrakchi F, Ahmed MJ, Khanday WA, Asif M, Hameed BH. Mesoporous carbonaceous material from fish scales as low-cost adsorbent for reactive orange 16 adsorption. J Taiwan Inst Chem Eng. 2017;71:47–54.
48. Meng Z, et al. Hierarchically porous cellulose nanocrystals for highly efficient removal of organic pollutants from water. ACS Appl Mater Interfaces. 2016;8(28):14204–13.
49. Ohwoavworhua FO, Okhamafe AO. Cellulose nanocrystals and nanofibrils obtained from corn straw by hydrolytic action of four acids: Particulate, powder and tablet properties. Drug Discov Anal. 2020;14(34):1–13.
50. Patel M, Kumar R, Kishor K, Mlsna T, Pittman CU, Mohan D. Pharmaceuticals of emerging concern in aquatic systems: Chemistry, occurrence, effects, and removal methods. Chem Rev. 2019;119:3510–73.

 

51. Patel AS, Lakshmibalasubramaniam S, Nayak B, Tripp C, Kar A, Sappati PK. Improved stability of phycobiliprotein within liposome stabilized by polyethylene glycol adsorbed cellulose nanocrystals. Int J Biol Macromol. 2020;163:209–18.
52. Patil S, Renukdas S, Patel N. Removal of methylene blue, a basic dye from aqueous solutions by adsorption using teak tree (Tectona grandis) bark powder. Int J Environ Sci. 2011;1(5):711–26.
53. Pires BC, Dutra FVA, Borges KB. Synthesis of mesoporous magnetic polypyrrole and its application in studies of removal of acidic, neutral, and basic pharmaceuticals from aqueous medium. Environ Sci Pollut Res. 2020;27(6):6488–504.
54. Pouran Pourhakkak, Taghizadeh A, Taghizadeh M, Ghaedi M, Haghdoust S. Fundamentals of adsorption technology. Elsevier; 2021. https://doi.org/10.1016/B978-0-12-818805-7.00001-1.
55. Rahman MM, Al Mamun MR, Islam MS, Hossain MA, Haque MM. Sulfuric acid hydrolyzed cellulose nanocrystals: Surface modification, characterization, and adsorption application. Carbohydr Polym. 2021;260:117778.
56. Segal L, Creely JJ, Martin AE, Conrad CM. An empirical method for estimating the degree of crystallinity of native cellulose. Text Res J. 1959;29(10):786–94.
57. Tang J, Zong L, Mu B, Kang Y, Wang A. Attapulgite/carbon composites as a recyclable adsorbent for antibiotics removal. Korean J Chem Eng. 2018;35(8):1650–61.
58. Tran HN, You SJ, Chao HP. Effect of temperature on biochar adsorption efficiency. Chem Eng J. 2017;308:904–13.
59. Wang J, Gao Y, Zhang H, Xu X. Adsorption of ciprofloxacin on cellulose nanocrystals: Kinetics and thermodynamics. Colloids Surf A. 2020;585:124142.
60. Wang J, Xu R, Huang M, Chen Z. Magnetic carbon nanocomposites for ciprofloxacin removal from water. J Hazard Mater. 2022;423:127009.
61. Wang J, Zhang Y, Cui W, Lu H. Structural evolution and adsorption properties of alkali-treated cellulose nanocrystals: A comparative study. Cellulose. 2020;27(3):1321–35.
62. Weber WJ, Morris JC. Kinetics of adsorption on carbon from solution. J Sanitary Eng Div. 1963;89(2):31–60.
63. Wu Q, Li Z, Hong H, Yin J, Wei H. Adsorption of tetracycline, sulfamethoxazole, and ciprofloxacin antibiotics onto biochar derived from agricultural residues: A comparison of kinetic, isotherm, and thermodynamic properties. Water Res. 2020;184:116164.
64. Xu R, Du H, Wang H, Zhang M, Wu M, Liu C, et al. Valorization of enzymatic hydrolysis residues from corncob into lignin-containing cellulose nanofibrils and lignin nanoparticles. Front Bioeng Biotechnol. 2021;9:677963.
65. Yousefi M, Mahmud S, Aziz A, Rahman MM. Removal of pharmaceutical compounds from water and wastewater using cellulose-based adsorbents: A review. Environ Technol Innov. 2021;24:101873.
66. Yousefi M, Mahmud S, Aziz A, Rahman MM. Utilization of rice husk-derived nanocellulose for wastewater treatment applications. J Environ Manag. 2022;304:114255.
67. Zhang L, Zhang M, Sillanpää M. Adsorption of ciprofloxacin from aqueous solution by modified silica particles: Mechanism, kinetics, and isotherms. J Hazard Mater. 2019;377:52–60.
68. Zhang L, Zhao X, Wang Y, Zhang H. Chitosan-graphene oxide composites for erythromycin removal: Kinetic and isotherm studies. Chem Eng J. 2021;405:126623.
69. Zhang W, Wang C, Zhang M, Lu W. Magnetic biochar adsorption of sulfamethazine: Temperature effects. Bioresour Technol. 2020;313:123729.
70. Zhao X, Wang Y, Li S, Chen Z. Biochar-based adsorbents for ciprofloxacin removal from water: Isotherm and kinetic modeling. Chemosphere. 2022;306:135681.
71. Zhao Y, Zhang L, Chen S, Wang Y. Adsorption behavior and mechanism of antibiotics onto activated carbon: A review. Chemosphere. 2022;307:135691.
72. Ioelovich M. Characterization of cellulose crystallinity using X-ray diffraction. Cellulose Chem Technol. 2015;49(7–8):7–8

 